Supplementary information: Quantitative theoretical analysis of the electrostatic force between a metallic tip and semiconductor surface in Kelvin probe force microscopy

Nobuyuki Ishida[1] and Takaaki Mano[1]

[1]*National Institute for Materials Science,*

1-2-1 Sengen, Tsukuba, Ibaraki 305-0047, Japan

```
C
C Output potential in the vacuum region
C
      WRITE(FILENAME,'("pot",I0.3,".dat")') IBIAS
      OPEN(unit=90,FILE=FILENAME)
      WRITE(90,*) RAD,SLOPE,sep,BIAS0,DELPHI
      WRITE(90,*) NV,NR,NS
      DO 522 I=0,NR,1
         II=I
         IF (II.EQ.0) II=1
         RSAV = R(II)
         IF (I.EQ.0) RSAV=-RSAV
         DO 521 J=1,NV,1
            WRITE(90,*) RSAV*SQRT(1.-(ETAT*J/NV)**2),J*DELV(II),
     &      VAC(1,II,J)
521      CONTINUE
      WRITE(90,*)
522   CONTINUE
      CLOSE(90)
```

FIG. S1: Scripts added to the line 345 in the ”semitip_v4.f” file to output the coordinates (r and z values) of grid points in the vacuum region and the electrostatic potential at each grid point.

```
1         number of sets of parameters to follow
1.00      shank slope (dimensionless) = tan (90-(theta/2)) where theta is shank opening angle
1.530     tip-sample separation (nm)
15.       tip radius (nm)
0.        radius of hemispherical protrusion at end of tip (nm)
0.850     contact potential (work function of tip relative to sample) (eV)
5.e17     donor concentration (cm^-3)
0.e17     acceptor concentration (cm^-3)
1.512     band gap (eV)
0.006     donor binding energy (eV)
0.028     acceptor binding energy (eV)
0.0635    conduction band effective mass
0.643     heavy hole effective mass
0.081     light hole effective mass
0.172     split-off hole effective mass
0.341     spin-orbit splitting (eV)
12.9      dielectric constant
78.       temperature (K)
0.00      modulation voltage (V)
0         semiconductor degeneracy indicator (=0 for nondegenerate,  =1 for degenerate)
1         inversion indicator (1 or 2 to suppress VB or CB occupation, 3 for both, 0 otherwise)
0         indicator for temperature dependence of surface state occupation (0=don't include it, 1=include it)
4.4e14    density of FIRST distribution of surface states (cm^-2 eV^-1)
0.756     charge neutrality level (eV)
0.25      FWHM for Gaussian distribution (use uniform distribution if zero) (eV)
1.180     centroid energies for Gaussian distribution (eV)
0.0       density of SECOND distribution of surface states (cm^-2 eV^-1)
0.0       charge neutrality level (eV)
0.0       FWHM for Gaussian distribution (use uniform distribution if zero) (eV)
0.0       centroid energies for Gaussian distribution (eV)
4.07      electron affinity of semiconductor
8.0       Fermi energy of tip (eV)
16        starting number of radial grid points
4         starting number of grid points into the vacuum
32        starting number of grid points into the semiconductor
0.5       scaling parameter for grid size
3         number of scaling steps for computation of potential
5000 3000 2000 2000    max no of iterations in each scaling step
1.e-4 1.e-4 1e-4 1e-4  convergence parameter for each scaling step
100000    size of table of charge densities (20000 high precision, 5000 low precision)
20        number of parallel wavevectors for computation of current (50 high precision, 20 low precision)
20        number of energies for computation of current (50 high precision, 20 low precision)
20        target expansion factor for integration of Schrodinger eqn (100 high precision, 10 low precision)
0.75      fraction of semiconductor depth to include in integration
```

TABLE I: The input parameters used for the electrostatic potential calculation in the SEMITIP.

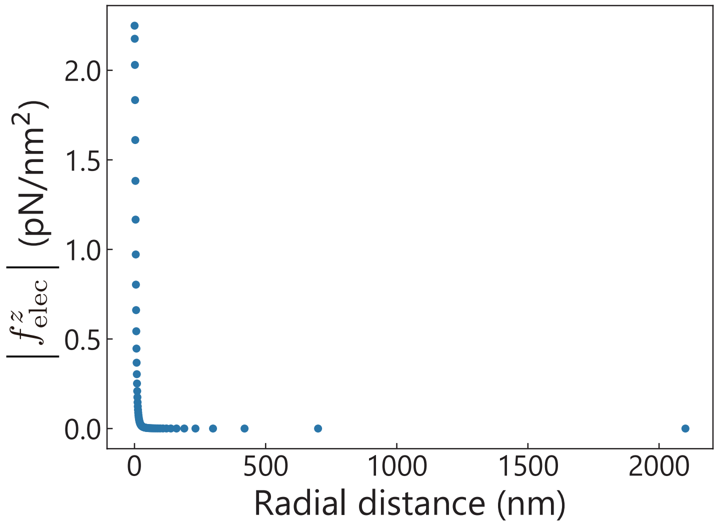

FIG. S2: z component of the electrostatic force per unit area (f^z_{elec}) acting on the tip surface plotted as a function of radial distance. The forces are expressed as absolute values. The range of r on the tip surface extended from 0 nm to approximately 2100 nm.

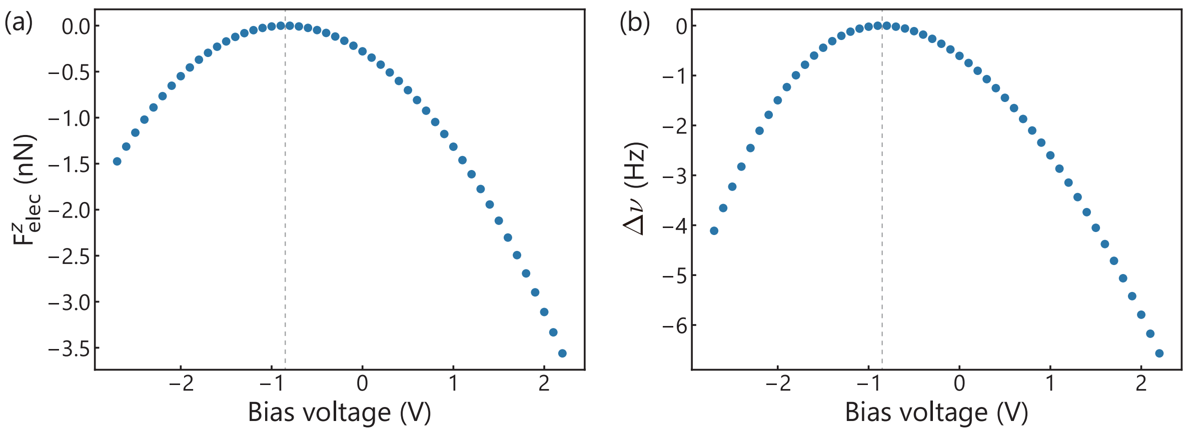

FIG. S3: $F^z_{\mathrm{elec}}(U)$ spectrum in (a) was converted into $\Delta\nu(U)$ spectrum in (b) using Eq. 2 in the main article. Both curves exhibited parabolic-like behavior, with the minimum of the absolute values appearing at the bias voltage corresponding to the input contact potential difference (CPD), as indicated by dashed vertical lines.

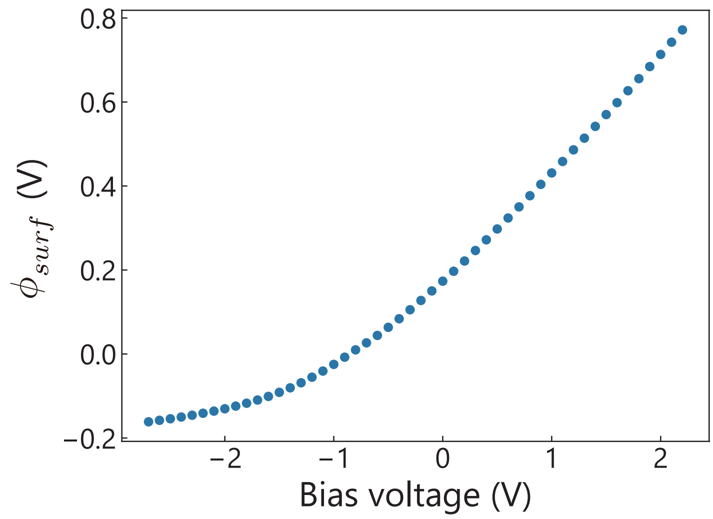

FIG. S4: Magnitude of tip-induced band bending (TIBB) as a function of bias voltage. The TIBB (ϕ_{surf}) was measured relative to the potential energy at a point far inside the semiconductor.

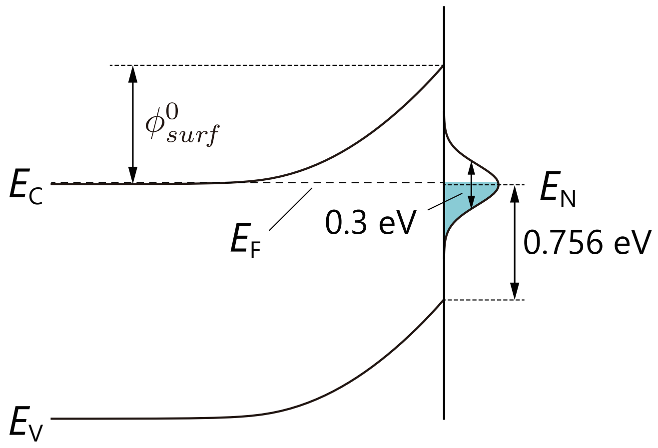

FIG. S5: Virtual surface states introduced to simulate the effect of Fermi level pinning. The surface states had a Gaussian type energy distribution, with the centroid energy located at the center of the band gap, i.e., 0.756 eV above the valence band edge. The full width at half maximum of the Gaussian distribution was 0.3 eV. The charge neutrality level E_N was located at the center of the Gaussian distribution. Due to the occupation of these states, the band bending occurred even in the absence of the tip near the semiconductor surface, a phenomenon referred to as Fermi level pinning.

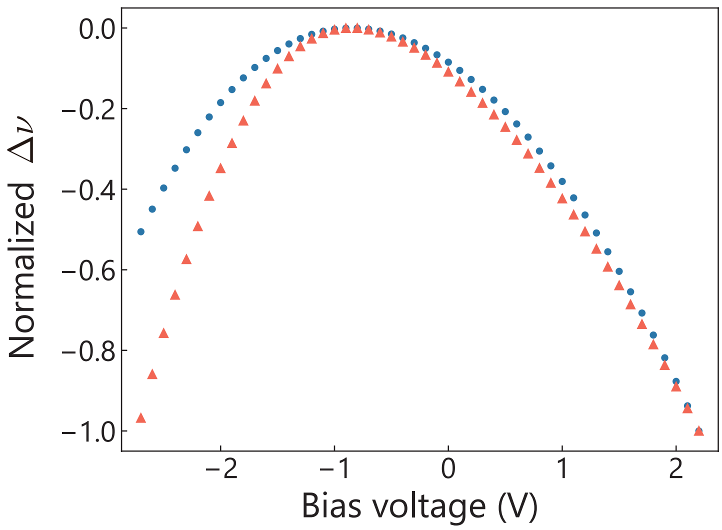

FIG. S6: Normalized $\Delta\nu(U)$ curves simulated with tip radii of 5 (solid circles) and 100 nm (solid triangles). The $\Delta\nu$ signals were normalized using the values at a bias voltage of 2.1 V. The normalization highlights the difference in curvature between the two curves across the entire bias range.

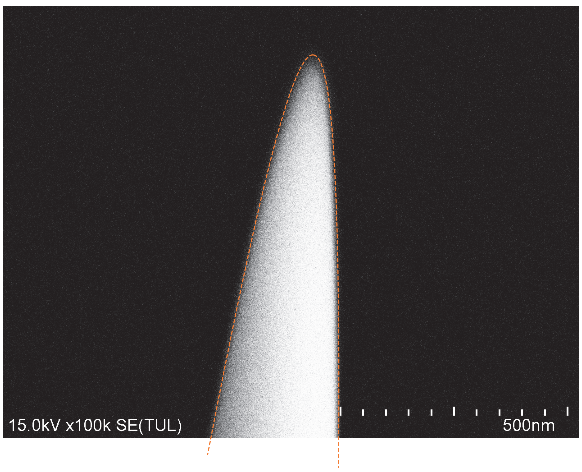

FIG. S7: Estimation of the radius of the W tip used in the experiment, performed using scanning electron microscopy (SEM). The contour of the tip apex was fitted with a hyperbolic curve (dashed line), using the tip radius and opening angle as fitting parameters. For the tip in the SEM image, a reasonable fit was obtained with a tip radius of 10 nm and an opening angle of 7 °.

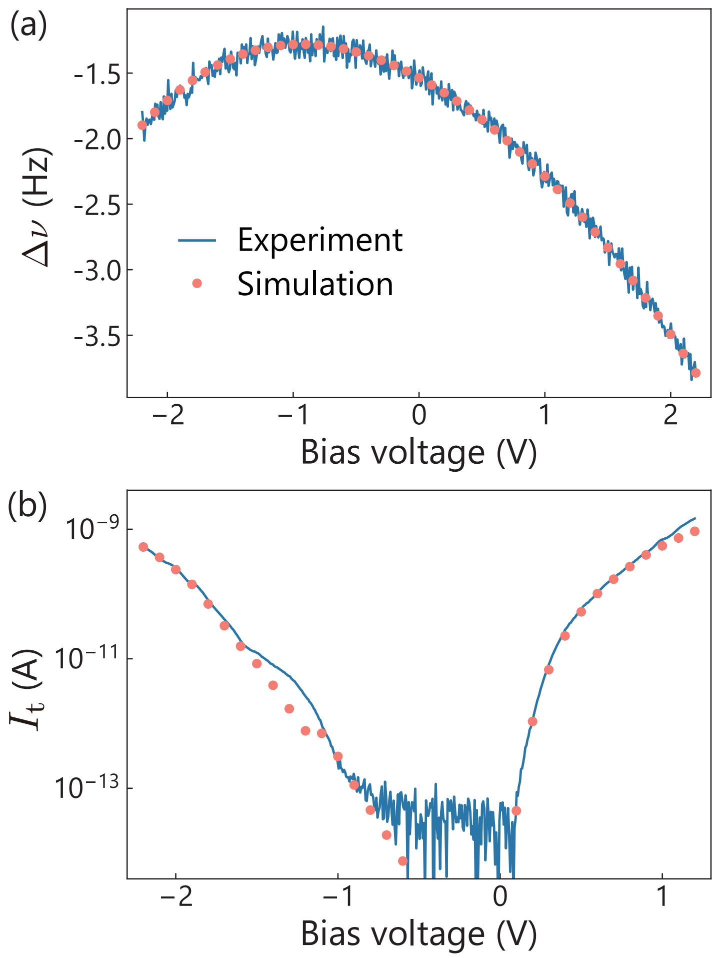

FIG. S8: Simultaneous fitting of the simulated tunneling current ($I_{\rm t}$) and $\Delta\nu$ data to the experiment. (a) Experimentally obtained $\Delta\nu(U)$ curve on the GaAs(110) surface (solid line). The oscillation amplitude of the qPlus sensor was 580 pm. Solid circles show the simulated $\Delta\nu(U)$ curve using parameter values of 10 nm, 1.53 nm, and 0.933 V for $R_{\rm tip}$, s, and CPD, respectively. The input CPD value was determined from curve fitting of a 9th-order polynomial to the $\Delta\nu(U)$ curve in the experiment. The values of $R_{\rm tip}$ and s were determined so that both simulated $\Delta\nu(U)$ and $I_{\rm t}(U)$ curves reproduced the experimental values. (b) Experimentally obtained $I_{\rm t}(U)$ spectrum at the same location as the $\Delta\nu(U)$ spectrum in (a) (solid line). The excitation of the qPlus sensor was turned off during tunneling spectroscopy. Solid circles represent the simulated $I_{\rm t}(U)$ spectroscopy data using the same parameter values as in the $\Delta\nu(U)$ spectroscopy case, except for s, which was set to 0.9 nm. The difference in s from the value used for the $\Delta\nu(U)$ simulation arose from the differences between the two spectroscopies in the values of the oscillation amplitude and the offset added in the tip-sample separations from the set point separation during the bias spectroscopy measurements.

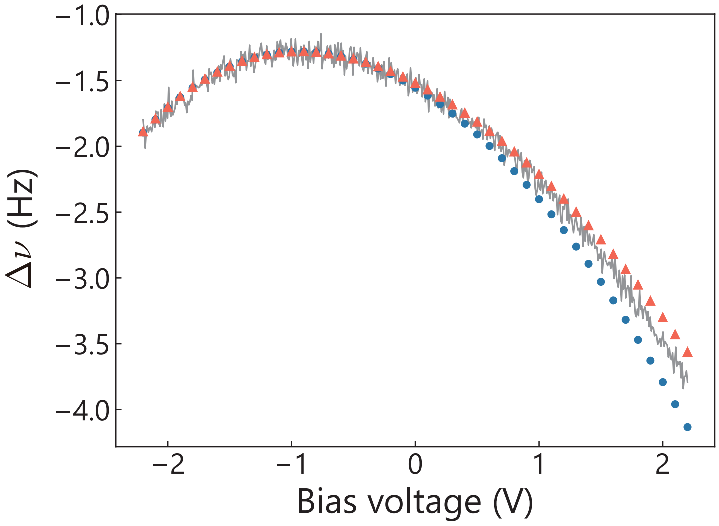

FIG. S9: The solid line shows the experimental $\Delta\nu(U)$ spectrum. The radius of the W tip used for this experiment was estimated from the curve fitting to be 10 nm. Blue solid circles and red solid triangles display the $\Delta\nu(U)$ curves calculated using tip radii of 5 nm and 15 nm, respectively. The coefficient term $(-\frac{\nu_0}{kA^2})$, treated as a fitting parameter (as discussed in the main article), was adjusted to ensure good fits to the experimental data on the left side of the inflection point. This parameter optimization resulted in deviations from the experiment on the right side of the inflection point. Conversely, when the parameter was adjusted to achieve good fits on the right side, deviations were observed on the opposite side.

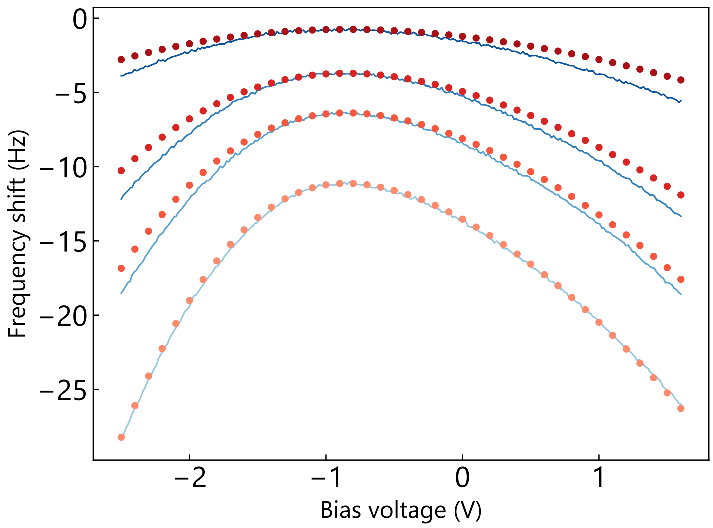

FIG. S10: Tip-sample separation dependence of the experimental $\Delta\nu(U)$ spectra (solid lines) obtained using a W tip with a large radius. The lift heights of the tip for the bias spectroscopy, relative to the tip-sample separation regulated by the STM feedback, were 0.1, 0.5, 1.0, and 3.0 nm. Solid circles represent $\Delta\nu(U)$ spectra from the simulations. To determine the parameters for the simulations, we first performed curve fitting of the simulation to the data obtained with a lift height of 0.1 nm. The tip radius estimated from the parameter optimization was 105 nm. Subsequently, we computed the $\Delta\nu(U)$ spectra by only changing the tip-sample separation according to the lift heights of the tip. While we achieved good agreement between theory and experiment for the data with a tip lift of 0.1 nm after the parameter optimization, slight deviations between theory and experiment were observed for the data of increased tip-sample separations.